JACS
JOURNAL OF THE AMERICAN CHEMICAL SOCIETY
Article
pubs.acs.org/JACS

Functionalization Based on the Substitutional Flexibility: Strong Middle IR Nonlinear Optical Selenides $AX^{II}_4X^{III}_5Se_{12}$

Hua Lin,[†] Ling Chen,*[,†] Liu-Jiang Zhou,[†,‡] and Li-Ming Wu*[,†]

[†]State Key Laboratory of Structural Chemistry, Fujian Institute of Research on the Structure of Matter, Chinese Academy of Sciences, Fuzhou, Fujian 350002, People's Republic of China

[‡]University of Chinese Academy of Sciences, Beijing 100039, People's Republic of China

Supporting Information

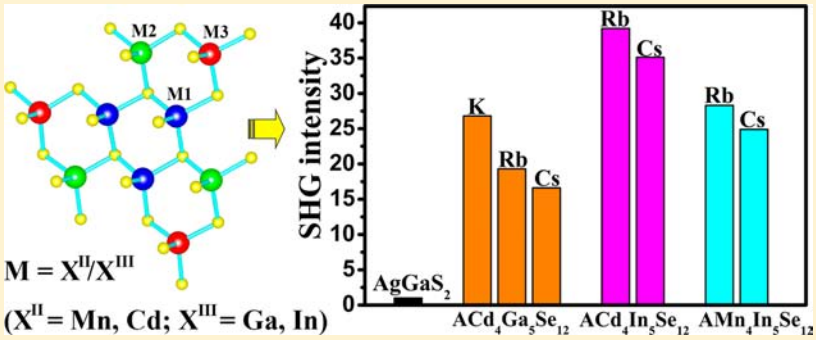

ABSTRACT: Seven nonlinear optical (NLO) active selenides in the middle IR region, $AX^{II}_4X^{III}_5Se_{12}$ (A = K^+–Cs^+; X^{II} = Mn^{2+}, Cd^{2+}; X^{III} = Ga^{3+}, In^{3+}) adopting the $KCd_4Ga_5S_{12}$-type structure, have been synthesized by high-temperature solid-state reaction of an elemental mixture with ACl flux. Their three-dimensional network structures are stacked by M_9Se_{24}-layers of vertex sharing MSe_4 tetrahedra, of which each center is jointly occupied by X^{II} and X^{III} atoms. Studies suggest that such tetrahedral building units can be regarded as the "multi-functional sites", on which the Cd^{2+}/Ga^{3+} pair gives rise to the coexistence of NLO and thermochromic properties, and the Mn^{2+}/In^{3+} pair leads to the coexistence of NLO and magnetic properties. The density functional theory (DFT) studies and the cutoff-energy-dependent NLO coefficient analyses reveal that such "multi-functional sites" contribute to the origin of the second harmonic generation (SHG) that is ascribed to the electronic transitions from the Se-4p states to the ns, np states of X^{II} and X^{III} atoms. Remarkably, title compounds show very strong SHG at an incident wavelength of 2.05 μm, roughly 16–40 times that of commercial $AgGaS_2$; among them, $ACd_4In_5Se_{12}$ (A = Rb, Cs) represents the strongest SHG among chalcogenides to date.

INTRODUCTION

Crystalline infrared nonlinear optical (NLO) materials are crucial in the modern IR laser frequency conversion technology that includes optoelectronic device, resource exploration, long-distance laser communication, etc., due to their advantage in the production of all solid-state, stable, portable laser devices.[1] However, high performance IR NLO crystals are rare, and each of the commercial crystals ($AgGaS_2$, $AgGaSe_2$, $ZnGeP_2$)[2,3] unfortunately suffers its own drawbacks, such as low laser damage threshold or two-photon absorption that hinder their application.[2,3] Therefore, the exploration and development of new IR NLO compounds is of broad scientific and technological importance.

Group 13-containing chalcogenides, in which the main group metal (e.g., Ga, In) always adopts an asymmetric tetrahedral coordination sphere that usually gives rise to the NLO properties, are interesting. Except the commercial $AgGaQ_2$ (Q = S, Se),[2] examples include many other compounds that are still in the experimental stage, such as $LiGaQ_2$,[4] $BaGa_4S_7$,[5] $BaGa_4Se_7$,[6] $AgGaGeS_4$,[7] $AgGaGe_3Se_8$,[8] $(K_3I)[SmB_{12}(GaS_4)_3]$,[9] $Li_2Ga_2GeS_6$,[10] $La_2Ga_2GeS_8$,[11] $Eu_2Ga_2GeS_7$,[11] Sm_4GaSbS_9,[12] $Ba_3CsGa_5Se_{10}Cl_2$,[13] $BaGa_2GeS_6$,[14] $Ba_{23}Ga_8Sb_2S_{38}$,[15] $LiGaGe_2Se_6$,[16] La_4InSbS_9,[17] and $Li_2In_2SiSe_6$.[18]

Among them, compounds with a general formula $AX^{II}_4X^{III}_5Q_{12}$ (adopting the $KCd_4Ga_5S_{12}$-type structure[19,20]) draw our attention. In the structure, "A" refers to a cation centering the large Q_{12} cuboctahedron that can be large alkali metal cation (K^+, Rb^+, or Cs^+); and divalent "X^{II}" and trivalent "X^{III}" jointly occupy each of the three crystallographic independent 9*b* sites (nominated as M site, i.e., M1, M2, and M3, hereafter). Recently, we discovered that $ACd_4Ga_5S_{12}$ exhibits not only very strong powder second harmonic generation (SHG) (with intensity 10 times larger than that of commercial $AgGaS_2$), but also thermochromic property. Also, the building unit MS_4 tetrahedron serves as the major NLO source according to the DFT analyses, and Cd atom is responsible for the thermochromism.[20] Stimulated by this, we

Received: July 24, 2013
Published: July 31, 2013

   dx.doi.org/10.1021/ja4074084 | J. Am. Chem. Soc. 2013, 135, 12914–12921

further consider it is possible to regard the MS_4 tetrahedron building unit with disordered M center as the "multi-functional sites", over which the atom disorder may provide an approach to modify the property. On the other hand, we regard the variations on the A and Q sites as the structure flexibility, which provides isostructural compounds to probe the structure–property relationship that can often be complicated or indirect in other systems.

Guided by this thought, we discovered 7 NLO active $KCd_4Ga_5S_{12}$-type selenides, $ACd_4Ga_5Se_{12}$ (A = K–Cs), $ACd_4In_5Se_{12}$ (A = Rb–Cs), and $AMn_4In_5Se_{12}$ (A = Rb–Cs), in this article. Among them, $ACd_4In_5Se_{12}$ (A = Rb, Cs) realizes the strongest powder SHG among selenides to date, about 35–40 times that of commercial $AgGaS_2$ at an incident laser wavelength of 2.05 μm at particle size of 46–74 μm. More interestingly, the substitutional flexibility enables their functionalization; the tetrahedral building unit serves as "multi-functional sites" that give rise to the NLO property that coexisted with either thermochromic or magnetic property depending on the identity of the X^{II}/X^{III} pairs. The syntheses, structure characterizations, property investigations, and DFT analyses are reported.

EXPERIMENTAL SECTION

Synthesis. Reactants were stored in a dry Ar-filled glovebox with controlled oxygen and moisture levels. Elements with purities higher than 99.99% were purchased from Sinopharm Chemical Reagent. The title compounds were synthesized from a mixture of ACl, X^{II} (Mn, Cd), X^{III} (Ga, In), and Se in a molar ratio of 3:4:5:12 with a slight excess of ACl as reactive flux. The reactants were loaded in a fused-silica tube under vacuum and then heated to 723 K in 10 h, kept at this temperature for 1 day, and then heated to 1273 K in 50 h, followed by a dwell period of 4 days, and subsequently cooled to 473 at 3 K/h before switching off the furnace. The products were washed first with distilled water to remove the excess ACl and chloride byproducts, and then dried with ethanol. After such a treatment, seven compounds were obtained as pure phases according to the powder X-ray diffraction (XRD) patterns shown in Figure 1b and Supporting Information Figure S1. Semiquantitative energy dispersive X-ray spectroscopy (EDX) analyses carried out on several single crystals revealed the presence of A, X^{II}, X^{III}, and Se in a ratio 1:4:5:12. For example, $K_{1.2(3)}Cd_{4.0(1)}Ga_{4.9(1)}Se_{12}$ (Supporting Information Figure S2) was close to $KCd_{4.0(3)}Ga_{5.0(3)}Se_{12}$ established by single-crystal diffraction data (Table 1, Supporting Information S1-1). No other element was detected. These compounds were stable in air for more than 1 year.

Single-Crystal X-ray Crystallography. Diffraction data were collected on a Rigaku Saturn70 CCD diffractometer or a Rigaku Saturn724 CCD diffractometer equipped with graphite-monochromated Mo Kα radiation (λ = 0.71073 Å) at 293 K. The data were corrected for Lorentz and polarization factors. Absorption correction was performed by the multiscan method.[21] The structure was solved by the direct method and refined by the full-matrix least-squares fitting on F^2 by SHELX-97.[22] Take $KCd_4Ga_5Se_{12}$ as an example; the initial refinement generated one K, four Se, and three "Cd" atoms with R values of R1 = 6.46% and wR2 = 15.68%. According to the EDX result, the compound should consist of Ga as well. Subsequently, Ga and Cd atoms were constrained to the same site (with identical coordinates and temperature factors) in SHELX.[20] Meanwhile, the Cd to Ga ratio was fixed as 4:5 to keep the charge balance, which also agreed with the EDX results. A check with the aid of PLATON[23] gave no hint for any higher symmetry. Finally, the structure refinement converged to R1 = 2.78%, wR2 = 5.43% with all atoms refined anisotropically, a Flack parameter of 0.07(2), and a formula of $KCd_{4.0(3)}Ga_{5.0(3)}Se_{12}$ (hereafter denoted as $KCd_4Ga_5Se_{12}$). Besides, the strong SHG effect of $KCd_4Ga_5Se_{12}$ substantiated the noncentrosymmetry of this compound. Nevertheless, we had also tried to refine the structure with input higher acentric space group of $R32$ or $R3m$. However, such treatments generated unreasonable temperature factors (0.007 or 0.090), short bond distance (less than 2.0 Å), unacceptable R values (R1/wR2 = 0.3338/0.6206), and large residual peaks (9.29 and −20.02 e Å^3). Therefore, the $R3$ space group was correct. The crystallographic data were listed in Table 1 and Supporting Information Table S1-2.

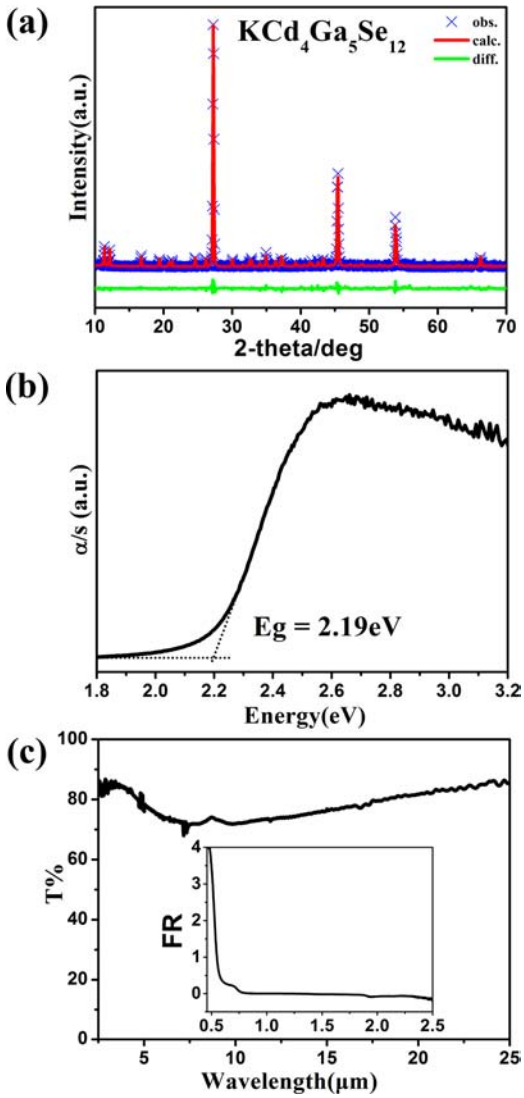

Figure 1. Property measurements on $KCd_4Ga_5Se_{12}$: (a) Experimental powder XRD (×, and the calculated (solid line), and difference (bottom) results of the GSAS refinements; impurity is not observed. (b) UV–vis diffuse-reflectance spectrum. (c) Reflection (inset) and FT-IR spectra.

Powder X-ray Diffraction. The XRD patterns were taken at room temperature on a Rigaku DMAX 2500 powder X-ray diffractometer by using Cu Kα radiation (λ = 1.5418 Å) at room temperature in the range of 2θ = 10–70° with a scan step width of 0.02°. Powder XRD data were analyzed using a profile fitting by a least-squares method employing the computer program GSAS implemented with EXPGUI.[24]

Elemental Analysis. EDX data were collected on a field emission scanning electron microscope (FESEM, JSM6700F) equipped with an energy dispersive X-ray spectroscope (EDX, Oxford INCA) on clean single-crystal surfaces.

Magnetic Susceptibility. The direct current magnetic susceptibility was measured on a Quantum Design MPMS-XL magnetometer at a field of 1000 Oe in the temperature range of 2–300 K. Hand-picked single crystals were ground to a fine powder to minimize the

dx.doi.org/10.1021/ja4074084 | J. Am. Chem. Soc. 2013, 135, 12914–12921

Table 1. Crystallographic Data and Refinement Details for $AX^{II}_4X^{III}_5Se_{12}$ (A = K−Cs; X^{II} = Mn, Cd; X^{III} = Ga, In)

	formula						
	$KCd_4Ga_5Se_{12}$	$RbCd_4Ga_5Se_{12}$	$CsCd_4Ga_5Se_{12}$	$RbCd_4In_5Se_{12}$	$CsCd_4In_5Se_{12}$	$RbMn_4In_5Se_{12}$	$CsMn_4In_5Se_{12}$
fw	1784.82	1831.19	1878.63	2056.69	2104.13	1826.85	1874.29
crystal system	trigonal						
crystal color	orange-red	orange-red	orange-red	black-red	black-red	black-red	black-red
space group	*R*3 (No. 146)						
a (Å)	14.362(5)	14.406(2)	14.4204(8)	14.8270(5)	14.864(5)	14.6793(9)	14.7202(8)
c (Å)	9.724(5)	9.769(2)	9.780(2)	10.0747(5)	10.102(5)	9.973(2)	10.004(2)
V (Å^3)	1737.1(2)	1755.6(4)	1761.3(3)	1918.1(2)	1932.9(2)	1861.1(3)	1877.2(3)
Z	3						
D_c (g/cm^3)	5.118	5.196	5.313	5.342	5.423	4.890	4.974
μ (mm^{-1})	28.339	29.928	29.300	26.634	25.946	26.057	25.335
GOF on F^2	1.077	0.999	1.012	1.081	1.096	1.051	1.014
R_1, wR_2 ($I > 2\sigma(I)$)[a]	0.0278, 0.0543	0.0254, 0.0412	0.0316, 0.0711	0.0292, 0.0685	0.0276, 0.0639	0.0306, 0.0598	0.0396, 0.0863
R_1, wR_2 (all data)	0.0307, 0.0548	0.0279, 0.0422	0.0350, 0.0729	0.0296, 0.0687	0.0279, 0.0641	0.0340, 0.0608	0.0461, 0.0893
largest diff. peak and hole (e/Å^3)	0.733, −0.640	0.858, −0.749	1.674, −1.878	1.693, −1.384	3.433, −0.986	0.932, −1.326	2.858, −1.829
absolute structure parameter	0.07(2)	−0.003(19)	0.02(2)	0.000(16)	0.000(16)	0.000(18)	0.00(3)

[a] $R_1 = \sum||F_o| - |F_c||/\sum|F_o|$, $wR_2 = [\sum w(F_o^2 - F_c^2)^2/\sum w(F_o^2)^2]^{1/2}$.

possible anisotropic effects and loaded into a gelatin capsule. The field-dependent magnetization was measured at 10 K via cycling the fields from −5 to +5 T. Data were corrected for the susceptibility of the container and for the diamagnetic contribution from the ion core.

Infrared and UV−Vis−NIR Diffuse Reflectance Spectra. The optical diffuse reflectance spectrum of powder sample was measured at room temperature using a Perkin-Elmer Lambda 900 UV−vis spectrophotometer equipped with an integrating sphere attachment and $BaSO_4$ as a reference over the range of 0.19−2.5 μm. The absorption spectrum was calculated from the reflection spectrum via the Kubelka−Munk function: $\alpha/S = (1 - R)^2/2R$, in which α was the absorption coefficient, S was the scattering coefficient, and R was the reflectance.[25] The IR data were measured by a Perkin-Elmer Spectrum one an FT-IR spectrophotometer in the range of 2.5−25 μm. Powder sample was ground with KBr and pressed into a transparent pellet for the measurement.

Powder Second Harmonic Generation (SHG) Measurements. Powder SHG measurements were performed on a modified Kurtz-NLO system using a 2.05 μm laser radiation.[26] The title compounds were ground and sieved in the range of 30−46, 46−74, 74−106, 106−150, and 150−210 μm, respectively, and ground $AgGaS_2$ single crystal sieved with the size range was used as a reference (1 × 1 × 2 cm^3 single crystals supplied from Anhui Institute of Optics and Fine Mechanics Chinese Academy of Sciences).

Electronic Structure Calculations. According to the $CsCd_4Ga_5Se_{12}$ single-crystal structure refinement results, Cd and Ga jointly shared each of the three 9*b* Wyckoff sites with Cd occupancies of about 0.50, 0.50, and 0.33. Nine configurations had been designed in the *P*1 symmetry, in which 12 Cd and 15 Ga atoms were randomly distributed over the 27 sites corresponding to the three Wyckoff 9*b* sites in the *R*3 structure as shown in Supporting Information Figure S7. Note these configurations were not exhaustive. According to the total energy, M7 was the most energy favorable configuration. Also, the electronic structures and density of states (DOS) were calculated on the basis of the M7 model. The *P*1 model of $CsCd_4In_5Se_{12}$ was built similarly. The geometrical optimization, electronic structures, and DOS of $CsCd_4Ga_5Se_{12}$ and $CsCd_4In_5Se_{12}$ were calculated by the Vienna ab initio simulation package VASP.[27a] The generalized gradient approximation (GGA)[27b] was chosen as the exchange-correlation functional, and a plane-wave basis with the projector augmented wave (PAW) potentials was used.[27c,d] The valence electrons included Cs 6s^1, Cd 4d^{10}5s^2, Ga 4s^{2}4p^1, In 5s^{2}5p^1, and Se 4s^{2}4p^4. In the geometrical optimization, an energy cutoff of 360 eV and a 3 × 3 × 3 Monkhorst-Pack *k*-point grid were employed. The atoms were allowed to relax until the forces on atoms were less than 0.02 eV/Å. In the static self-consistent-field calculation, a plane-wave cutoff energy of 450 eV and the threshold of 10^{-5} eV were set. The *k* integration over the Brillouin zone was performed by the tetrahedron method[27e] using a Monkhorst−Pack grid, 5 × 5 × 6 for $CsCd_4Ga_5Se_{12}$ and $CsCd_4In_5Se_{12}$, and 17 × 17 × 17 for $AgGaS_2$, respectively. The Fermi level (E_f = 0 eV) was selected as the reference of the energy.

In the optical property calculations, same plane-wave cutoff energy and Monkhorst−Pack grid were utilized; scissors operators of 1.04, 0.63, and 1.79 eV were applied for $CsCd_4Ga_5Se_{12}$, $CsCd_4In_5Se_{12}$, and $AgGaS_2$, respectively. The dielectric function $\varepsilon(\omega)$, adsorption coefficient $\alpha(\omega)$, reflectance coefficient $R(\omega)$, and refractive index $n(\omega)$ were obtained via the Kramers−Kroning transform.[28] The static and dynamic second-order nonlinear susceptibilities $\chi^{abc}(-2\omega, \omega, \omega)$ were calculated on the basis of the electronic structure according to the length-gauge formalism by Aversa and Sipe.[29] Considering the relationship between *R*3 and *P*1 symmetry, and the restriction of Kleinman's symmetry,[30] the χ_{11}, χ_{15}, χ_{22}, χ_{33} and the corresponding second-order coefficient d_{11}, d_{15}, d_{22}, d_{33} of the *P*1 model were studied to probe those in the *R*3 symmetry (details in the Supporting Information).

RESULTS AND DISCUSSION

Synthesis. $ACd_4Ga_5Se_{12}$ (A = K−Cs), $ACd_4In_5Se_{12}$, and $AMn_4In_5Se_{12}$ (A = Rb−Cs) have been obtained as pure phases via high-temperature solid-state reactions. The phase purity is confirmed by the powder XRD patterns (Figure 1a and Supporting Information Figure S1). The EDX analyses of several crystals confirm the presence of each component, which agree well with the single-crystal refinement results. Attempts for proposed "$KMn_4In_5Se_{12}$" and "$KCd_4In_5Se_{12}$" only yield ternary Mn_2InSe_4 and Cd_2InSe_4, respectively. Several attempts for the Na analogue also failed. The reason may be related to the prerequisite that the A cation in an $AX^{II}_4X^{III}_5Se_{12}$ should be large enough to hold the anionic large Se_{12} cuboctahedral cavity.

Crystal Structure. Single X-ray crystal diffraction data reveal that $ACd_4Ga_5Se_{12}$, $ACd_4In_5Se_{12}$, and $AMn_4In_5Se_{12}$ adopt the $KCd_4Ga_5S_{12}$-type structure[19,20] (Figure 2 and Table 1). The major structure motif is the 3D network (Figure 2a) stacked by a 2D M_9Se_{24}-layer (Figure 2b) along the *c* axis. Each M_9Se_{24} building block consists of vertex sharing $M1Se_4$ (blue), $M2Se_4$ (green), and $M3Se_4$ (red) tetrahedra (Figure 2c). The M site is disordered by X^{II} and X^{III} atoms, such as Cd/Ga, Cd/In, and Mn/In pairs with occupancies of 28−58% Cd, 42−72% Ga,

dx.doi.org/10.1021/ja4074084 | J. Am. Chem. Soc. 2013, 135, 12914−12921

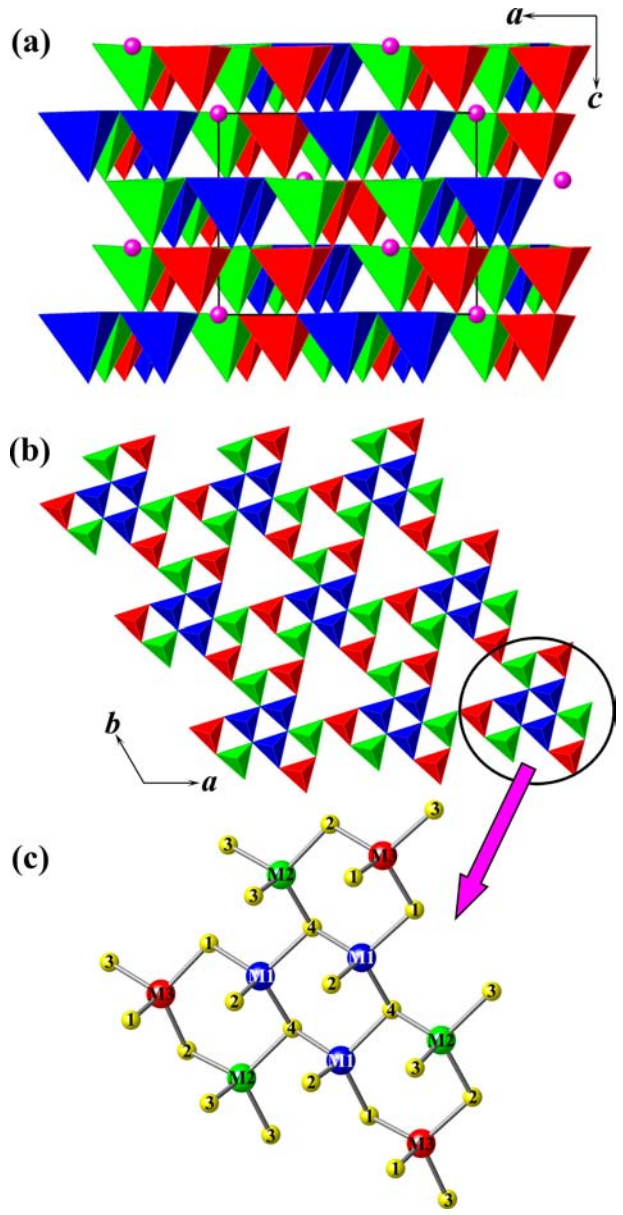

Figure 2. (a) Crystal packing structure of $AX^{II}_4X^{III}_5Se_{12}$ viewed down the *b*-axis with the unit cell marked. Purple, A; tetrahedron, MSe_4 (M is disordered by X^{II} and X^{III} atoms); blue, $M1Se_4$; green, $M2Se_4$; red, $M3Se_4$. (b) A single 2D M_9Se_{24}-layer perpendicular to the *c* direction. (c) The asymmetric building unit, M_9Se_{24}, with atom number marked. Yellow: Se.

44−69% In, or 31−56% Mn as listed in Table S1 (Supporting Information).

Interestingly, the ionic radii difference between X^{II} and X^{III} atoms affects their distribution pattern over the M sites. For instance, in cases of $ACd_4Ga_5Q_{12}$ (Q = Se, S) with larger $r(X^{II})/r(X^{III})$ = 1.44 ($Cd^{2+}_{CN=4}$, 0.78 Å and $Ga^{3+}_{CN=4}$, 0.47 Å),[31] the occupancy of X^{II} follows a trend of M1 > M2 > M3 (Supporting Information Tables S1-1, -4). In case of $ACd_4In_5Se_{12}$ with smaller $r(X^{II})/r(X^{III})$ = 1.25 ($Cd^{2+}_{CN=4}$, 0.78 Å, $In^{3+}_{CN=4}$, 0.62 Å),[31] X^{II} distributes nearly evenly at M1 ≈ M2 ≈ M3 (Supporting Information Table S1-2). Differently, the $r(X^{II})/r(X^{III})$ = 1.07 ($Mn^{2+}_{CN=4}$, 0.66 Å, $In^{3+}_{CN=4}$, 0.62 Å)[31] of $AMn_4In_5Se_{12}$ is smaller than that of $ACd_4Ga_5Q_{12}$, and the occupancy of X^{II} follows the same trend of M1 > M2 > M3 as in $ACd_4Ga_5Q_{12}$ (Supporting Information Table S1-3). Despite the different distribution of X^{II}, the overall stoichiometry of $A^+X^{II}_4X^{III}_5(Se^{2-})_{12}$ is fixed because of the charge balance requirement. The cationic A centers the Se_{12} cuboctahedron (Figure S3, Supporting Information), and the identity of the alkali metal on going from K^+, Rb^+, to Cs^+ does not affect significantly the occupancy on the 9*b* site (Supporting Information Table S1), but affects the NLO property as discussed below (Tables 2, 3).

Table 2. Measured Optical Properties for $AX^{II}_4X^{III}_5Se_{12}$ (A = K−Cs; X^{II} = Mn, Cd; X^{III} = Ga, In)

	experimental		
$AX^{II}_4X^{III}_5Se_{12}$	SHG intensity[a]	trans. region (μm)[b]	E_g (eV)
$KCd_4Ga_5Se_{12}$	26.8	0.75−25	2.16
$RbCd_4Ga_5Se_{12}$	19.3	0.72−25	2.19
$CsCd_4Ga_5Se_{12}$	16.6	0.70−25	2.21
$RbCd_4In_5Se_{12}$	39.2	0.87−25	1.57
$CsCd_4In_5Se_{12}$	35.1	0.85−25	1.62
$RbMn_4In_5Se_{12}$	28.3	0.96−25	1.76
$CsMn_4In_5Se_{12}$	24.9	0.94−25	1.79

[a]Relative to the commercial $AgGaS_2$ (46−74 μm) with $\lambda_{incident}$ = 2.05 μm. [b]Measured on the polycrystalline sample.

Properties. The magnetic susceptibility of compound $CsMn_4In_5Se_{12}$ at an applied field of 1000 Oe in the temperature range 2−300 K obeys the Curie−Weiss law above 70 K (Figure 3a). The least-squares method fit with the equation $\chi_M = C/(T - \theta)$ generates C = 4.14 emu K/mol and θ = −44.21 K. The effective magnetic moment ($\mu_{eff} \approx 5.76\ \mu_B$ per Mn^{2+}) obtained according to the equation $\mu_{eff} = (7.997C)^{1/2}\mu_B$[32] deviates slightly from the theoretical value for a high-spin Mn^{2+} spin (5.92 μ_B per Mn^{2+}). The large negative θ suggests significant antiferromagnetic (AF) interactions between the Mn^{2+} cations (the nearest Mn−Mn distance is 4.04 Å). Below 70 K, the inverse magnetic susceptibility (Figure 3a) shows a gradual decrease, indicating a ferrimagnetic or a spin-canting AF behavior. As shown in Figure 3b, the nonlinear behavior of the field dependence of magnetization at 10 K reveals the presence of a net magnetic moment. Yet the field dependence of the magnetization does not follow a Brillouin curve, and the magnetization increases to 0.75 Nβ without a saturation up to 5 T, much less than the common value of 20 Nβ for four Mn^{2+} centers, which suggests a spin-canted AF interaction between the magnetic ions. Such a behavior is also observed in $Na_4Mn_3(PO_4)(P_2O_7)$, $[Mn(bphz)(N_3)_2]_n$, and $Sm_2Mn_3Sb_4S_{12}$.[33]

The IR spectra and diffuse-reflectance UV/vis/near-IR spectra of the seven title compounds (measured on polycrystalline samples) indicate broad transparent regions of 0.89−25 μm (Supporting Information Figures S4,S5) that run across the two important atmospheric transparent windows (3−5 and 8−14 μm).[34] The IR transparency is comparable with that of commercial $AgGaS_2$ (0.15−23 μm, Supporting Information Figure S6), and those of $BaGa_4Se_7$ (up to 18 μm)[6] and $Ba_3AGa_5Se_{10}Cl_2$ (A = Cs, Rb, and K) (0.65−25 μm).[13]

In agreement with their orange-red or black-red colors, the optical band gaps are measured to be approximately 2.20, 1.60, and 1.80 eV for $ACd_4Ga_5Se_{12}$, $ACd_4In_5Se_{12}$, and $AMn_4In_5Se_{12}$ (Table 2 and Supporting Information Figure S4). These gaps are smaller than those of $AgGaS_2$ (2.56 eV, Supporting Information Figure S8a), $BaGa_4S_7$ (3.54 eV),[5] and $BaGa_4Se_7$

dx.doi.org/10.1021/ja4074084 | J. Am. Chem. Soc. 2013, 135, 12914−12921

Table 3. Property Comparison between Selected $AX^{II}_4X^{III}_5Q_{12}$ and Commercial $AgGaS_2$

	$CsCd_4In_5Se_{12}$	$CsCd_4Ga_5Se_{12}$	$CsCd_4Ga_5S_{12}$[20]	$AgGaS_2$
SHG coeff. (pm/V) at 2.05 μm[a]	d_{11} = 48.6	d_{11} = 26.8	d_{11} = 14.6	d_{36} = 18.2
	d_{15} = 45.7	d_{15} = 23.7	d_{15} = 13.9	
	d_{22} = 43.0	d_{22} = 22.0	d_{22} = 12.2	
	d_{33} = 81.6	d_{33} = 42.1	d_{33} = 26.4	
absorp. edge (μm)	$0.85_{(obs)}$[b]	$0.70_{(obs)}$[b]	$0.42_{(obs)}$[b]	$0.60_{(obs)}$[b]
	$0.73_{(cal)}$[a]	$0.54_{(cal)}$[a]	$0.30_{(cal)}$[a]	$0.46_{(cal)}$[a]
trans. range (μm)	0.85−25[b]	0.70−25[b]	0.42−25[b]	0.60−23[b]
E_g (eV)	$1.62_{(obs)}$[b]	$2.21_{(obs)}$[b]	$3.09_{(obs)}$[b]	$2.56_{(obs)}$[b]
	$0.99_{(cal)}$[a]	$1.17_{(cal)}$[a]	$1.89_{(cal)}$[a]	2.70[2]
static birefringence[a]	0.01	0.014	0.003	0.039
average refractive index at 2.05 μm[a]	2.55	2.51	2.42	2.49
average static dielectric constant[a]	6.69	6.30	5.86	6.15

[a]Calculated value. See more details in the Supporting Informaiton. [b]Measured on ground single crystals.

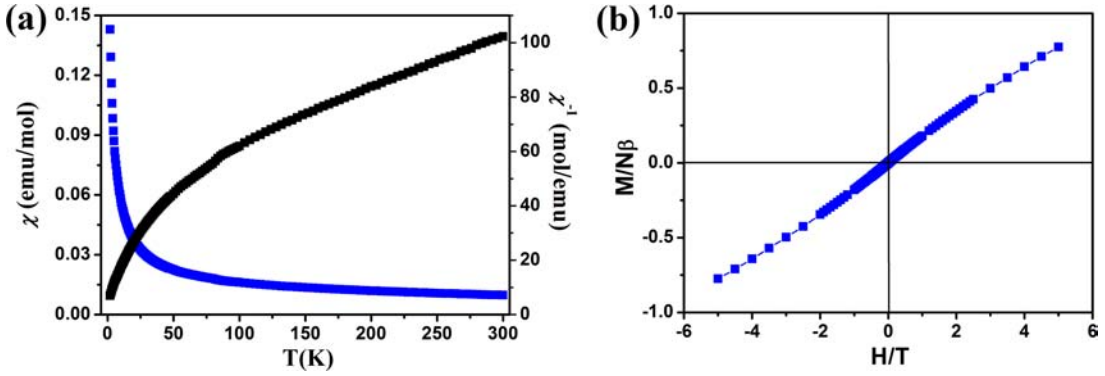

Figure 3. (a) Temperature dependence of the molar magnetic susceptibility (χ; blue) and the inverse molar magnetic susceptibility (χ^{-1}; black) for $CsMn_4In_5Se_{12}$ in a magnetic field of 1000 Oe. (b) Field dependence of magnetization of $CsMn_4In_5Se_{12}$ measured by cycling the field between +5 and −5 T at 10 K.

(2.64 eV),[6] but wider than those of $AgGaSe_2$ (1.8 eV)[35] and $ZnGeP_2$ (1.75 eV),[3] which indicates that these compounds may carry laser-induced damage threshold comparable to that of the commercial materials.

NLO Properties. The powder SHG have been measured using the Kurtz and Perry method with 2.05 μm Q-switch laser and $AgGaS_2$ as a reference. The particle size versus the SHG intensity curve (Figure 4a) indicates a non phase-matchable nature[5,36] with the peak intensity realized at the particle size of 46−74 μm (Figure 4b, Table 2). Remarkably, $ACd_4In_5Se_{12}$ (A = Rb, Cs) shows the highest intensity among chalcogenides to data, 35−40 times that of commercial $AgGaS_2$, stronger than those of $Ba_{23}Ga_8Sb_2S_{38}$, 22×;[15] $CsCd_4Ga_5S_{12}$, 10×;[20] Sm_4GaSbS_9, 3.8×;[12] La_4InSbS_4, 1.5×;[17] and $Eu_2Ga_2GeS_7$, 1.6×,[11] but weaker than that of the chalcohalide $Ba_3CsGa_5Se_{10}Cl_2$, 100 × $AgGaS_2$.[13] Note that for the SHG maxima peak at different particle sizes, if compared at the same size of 46−74 μm, the SHG intensity of $ACd_4In_5Se_{12}$ is stronger than that of $Ba_3CsGa_5Se_{10}Cl_2$ (14 × $AgGaS_2$).[13] As shown in Table 2, the SHG intensities of other members are strong too, 16−28 times that of $AgGaS_2$. The SHG intensities of the title compounds increase as the band gaps decrease, and the identity change of alkali metal A also influences the SHG intensity. Similar alkali metal effect has been found in $ACaCO_3F$[37] and $A_4GeP_4Se_{12}$.[38] The powder SHG, band gap, and transparency data suggest the title compounds as promising candidates as high performance IR NLO materials.

Electronic Structures. The electronic band structures reveal direct band gaps of 1.17 and 0.99 eV, for $CsCd_4Ga_5Se_{12}$ and $CsCd_4In_5Se_{12}$, respectively (Figure S7 in the Supporting Information). These values are smaller than the measured 2.21 and 1.62 eV due to the discontinuity of the exchange-correlation potential that underestimates the band gap in semiconductors and insulators.[39] The calculated total and partial densities of states of $CsCd_4Ga_5Se_{12}$ and $CsCd_4In_5Se_{12}$ are similar in the energy distribution of the eigenstates (Figure 5). The Cs-6s electronic states mainly lie in the energy region above 4.0 eV with a very small contribution in the top of valence band (VB) and bottom of conduction band (CB), indicating that Cs occurs as a cation that provides charge balance to the counteranion $[Cd_4X^{III}_5Se_{12}]^-$. The electrostatic interactions between the Cs cations and the polyanions contribute to stabilize the $AX^{II}_4X^{III}_5Se_{12}$ structure. In the VB region below the Fermi level, the Se-4p states dominating the VB-1 region are mixing with minor Cd-5s, Cd-5p, Cd-4d, and Ga-4p/In-5p states. Above the Fermi level, the CB-1 region is derived mainly from the Se-4p and Ga-4s/In-5s states mixing with small amounts of Cd-5s and Ga-4p/In-5p states. Therefore, the band gap absorptions are mainly ascribed to the charge transitions from the Se-4p states to Ga-4s/In-5s, Ga-4p/In-5p, and Cd-5s states. Similarly, the band gap absorption of $CsCd_4Ga_5S_{12}$ is mainly determined by the charge transitions from the S-3p states to Ga-4s, Ga-4p, and Cd-5s.[20] Thus, the band gap difference $AM^{II}_4M^{III}_5Q_{12}$ comes from the Se-4p and S-3p energy difference. Because the Se-4p is higher in energy than S-3p, the E_g of $AM^{II}_4M^{III}_5Q_{12}$ decreases on going from S to Se.

dx.doi.org/10.1021/ja4074084 | J. Am. Chem. Soc. 2013, 135, 12914−12921

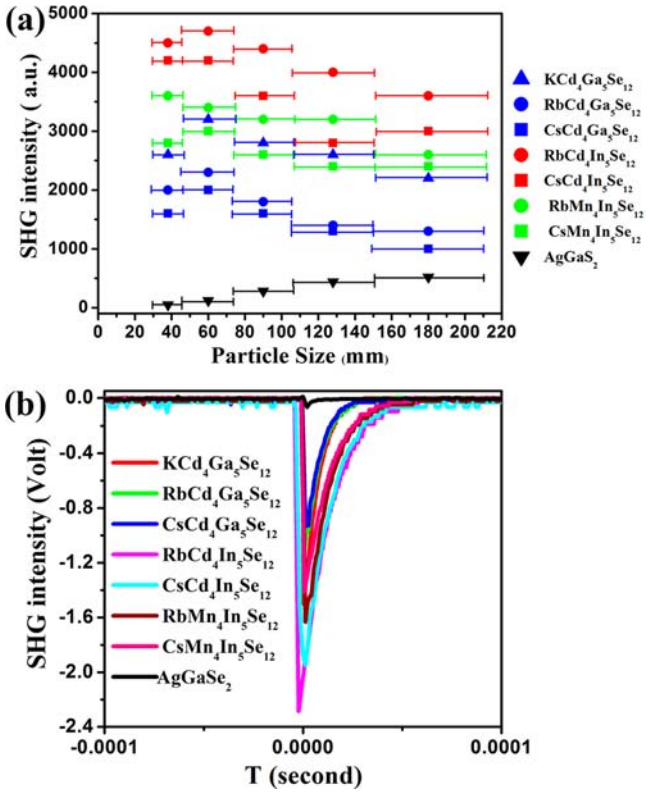

Figure 4. (a) Phase-matching curves, that is, particle size versus SHG response, for $AX^{II}_4X^{III}_5Se_{12}$ and $AgGaS_2$ (as reference). (b) Oscilloscope traces of SHG signals of $AX^{II}_4X^{III}_5Se_{12}$ and $AgGaS_2$ (reference) in the particle size of 46−74 μm.

Theoretical Analyses of the Optical Properties. The frequency-dependent dielectric function has been calculated (Supporting Information Figure S9). The onset to the $\varepsilon_2(\omega)$ curve reflects the band gap energy, which agrees with the experimental observations in principle. Besides, birefringence (Δn), absorption coefficient α and reflectivity R (Supporting Information Figures S10−S13) are also investigated. Several key parameters are summarized in Table 3, indicating that the calculations agree with the experimental observations. The static Δn values of $CsCd_4Ga_5Se_{12}$ and $CsCd_4In_5Se_{12}$ are 0.014 and 0.01, respectively, both larger than that of $CsCd_4Ga_5S_{12}$ (0.003),[20] but smaller than that of $AgGaS_2$ (0.039) (Supporting Information Figure S9). The relatively small Δn value in the IR region indicates a non phase-matchable behavior, which agrees with our experimental observation. However, larger Δn values in other energy regions are suggested for these compounds, indicating possible phase-matchable behavior in those spectrum regions.

As shown in Figure 6 and Table 3, the calculated SHG coefficients d_{11}, d_{15}, d_{22}, and d_{33} for $CsCd_4Ga_5Se_{12}$ and $CsCd_4In_5Se_{12}$ are larger than that of $AgGaS_2$ (d_{36} (2.05 μm) = 18.2 pm/V) at the wavelength of 2.05 μm (i.e., 0.61 eV). The calculated d_{ij} values of $CsCd_4Ga_5Se_{12}$ and $CsCd_4In_5Se_{12}$ are 1.6 and 3.1 times larger than that of $CsCd_4Ga_5S_{12}$,[20] which are in accordance with the experimental SHG intensity observations (1.7 or 3.5 times stronger than $CsCd_4Ga_5S_{12}$[20] at 46−74 μm with $\lambda_{incident}$ = 2.05 μm) (Table 2).

The origin of the SHG response has been investigated following the method in the literature[36b,40] via the cutoff-energy-dependent SHG coefficient according to the length-gauge formalism.[28] The cutoff-energy-dependent d_{33} shown in Figure 7 indicates that VB-1 and CB-3 regions contribute mainly to such an SHG coefficient. The DOS of $CsCd_4Ga_5Se_{12}$ shown in Figure 5 reveals that the VB-1 is dominated by Se-4p states hybridized with a small amount of Cd-5s, Cd-5p, Cd-4d, and Ga-4p, and CB-3 is mainly contributed from Se-4p and Ga-4p states mixing with small amounts of Cd-5p. A similar contribution is found for $CsCd_4In_5Se_{12}$ (Figure 7b). These results reveal that the overall SHG efficiency should be mostly influenced by Se-4p, Cd-5s, Cd-5p, and Ga-4p/In-5p states. Consequently, the SHG response may be ascribed to the electronic transitions from Se-4p, to Cd-5s, Cd-5p, and Ga-4p/In-5p states. Similarly, the SHG origin of $CsCd_4Ga_5S_{12}$ is ascribed to the electronic transitions from S-3p, to Gd-4p and Ga-4p.[20] Because of the decrease of E_g on going from S to Se, the SHG intensity increases. This agrees well with the SHG coefficient calculations.

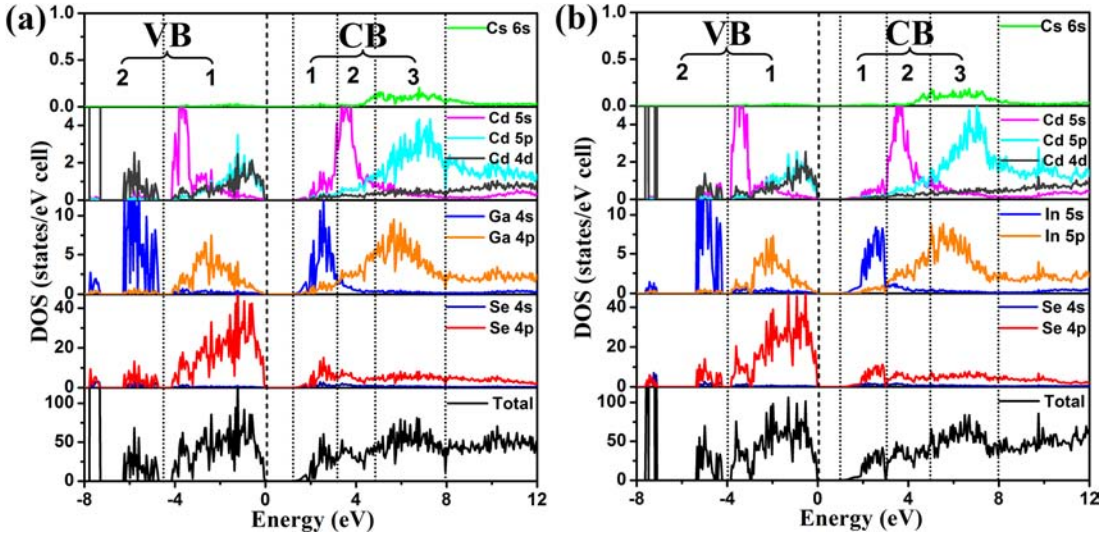

Figure 5. Total and partial densities of states of (a) $CsCd_4Ga_5Se_{12}$ and (b) $CsCd_4In_5Se_{12}$. Dashed line, E_F; dotted line, different regions in VB and CB.

dx.doi.org/10.1021/ja4074084 | J. Am. Chem. Soc. 2013, 135, 12914−12921

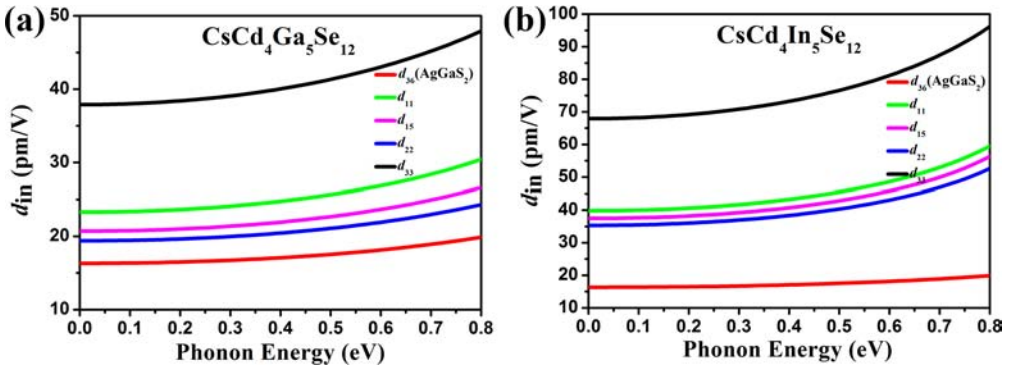

Figure 6. Calculated frequency-dependent SHG coefficients for (a) $CsCd_4Ga_5Se_{12}$ and (b) $CsCd_4In_5Se_{12}$. Those of $AgGaS_2$ are shown as a reference (red line).

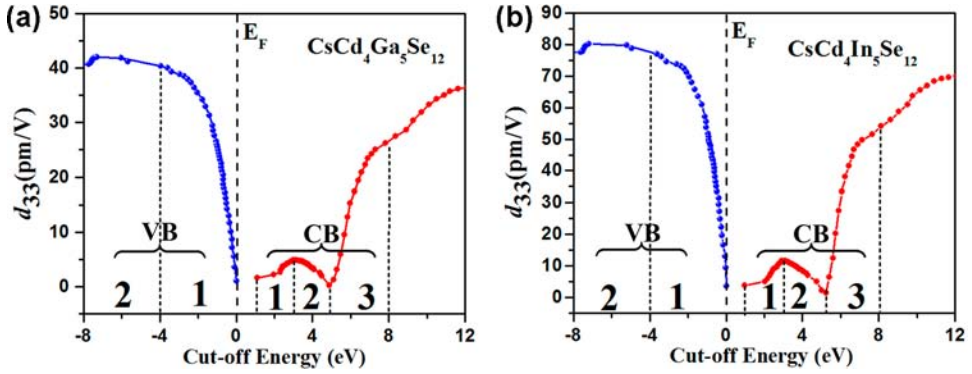

Figure 7. The cutoff-energy-dependent static SHG coefficients for (a) $CsCd_4Ga_5Se_{12}$ and (b) $CsCd_4In_5Se_{12}$. Dashed line, E_F; dotted line, different regions in VB and CB.

The results listed in Table 3 reveal that the SHG coefficient of $CsCd_4X^{III}{}_5Q_{12}$ (X^{III} = Ga, In; Q = S, Se) increases on going from Ga to In and from S to Se, which points out an experimental pathway to enhance the NLO response. This agrees well the general accepted knowledge that decreasing band gap is a major approach to enhance the magnitude of the SHG coefficient, because the major orbital determining the SHG process also determines the VB top and CB bottom as discussed above. Of course, the band gap decrease will lead to other unwanted effects, such as reduction of the laser damage threshold, narrowing of the transparency range, etc. To develop a new NLO material is to find the optimal balance among these criteria.

On the basis of the discussion on $ACd_4Ga_5Se_{12}$ (A = K−Cs), $ACd_4In_5Se_{12}$ (A = Rb−Cs), $AMn_4In_5Se_{12}$ (A = Rb−Cs), and $ACd_4Ga_5S_{12}$ (A = K−Cs),[20] it is rational to regard the MQ_4 building unit (centered by disordered bivalent X^{II} and trivalent X^{III} atoms) as the "multi-functional sites", on which X^{II} and X^{III} both contribute to the NLO property, and X^{II} is also responsible for the coexisting thermochromatic or magnetic properties. It is worth pointing out that the NLO, thermochromatic, and magnetic properties are measured independently. Are they coupled? It remains an unknown yet very interesting question to be explored.

CONCLUSION

In summary, seven NLO active $AX^{II}{}_4X^{III}{}_5Se_{12}$ selenides, $ACd_4Ga_5Se_{12}$, $ACd_4In_5Se_{12}$, and $AMn_4In_5Se_{12}$ (A = K−Cs), have been discovered by a modified reactive flux method. Interestingly, the M sites disordered by bivalent X^{II} and trivalent X^{III} metals can be regarded as the "multi-functional sites", on which the Cd^{2+}/Ga^{3+} pair gives rise to the coexistence of NLO and thermochromism properties, and the Mn^{2+}/In^{3+} pair leads to the combination of NLO and magnetic properties. The DFT studies and the cutoff-energy-dependent NLO coefficient analyses reveal that the "multi-functional sites" are responsible for the SHG origin that is ascribed to the electronic transitions from the Se-4p states to the ns and np states of X^{II} and X^{III} atoms. Remarkably, all of these compounds show very strong powder IR SHG at an incident wavelength of 2.05 μm, roughly 16−40 times that of commercial $AgGaS_2$; among them, $ACd_4In_5Se_{12}$ (A = Rb, Cs) represents the strongest powder SHG among chalcogenides to date (35−40 times that of commercial $AgGaS_2$) at the particle size of 46−74 μm. These features together with several other key parameters (transparency, band gap) make them promising candidates as a new NLO material working in the IR regions. The experimental results suggest the functionalization of these materials is achieved via taking advantage of the substitutional flexibility. This work will shed useful light on the future property-oriented design synthesis of novel materials.

ASSOCIATED CONTENT

Supporting Information

Additional crystallographic data, CIF files, XRD patterns, reflection and FT-IR spectra, UV diffuse reflectance spectra, calculation results including dielectric functions, refractive index, reflectivity, absorption coefficient, and birefringence, together with additional tables and figures. This material is available free of charge via the Internet at http://pubs.acs.org.

dx.doi.org/10.1021/ja4074084 | J. Am. Chem. Soc. 2013, 135, 12914−12921

AUTHOR INFORMATION

Corresponding Author

chenl@fjirsm.ac.cn; liming_wu@fjirsm.ac.cn

Author Contributions

H. Lin, L. Chen performed the experiments, L.-M. Wu, L.-J. Zhou performed the theoretical analyses. H. Lin, L. Chen and L.-M. Wu conceived the experiments, analyzed the results and wrote and edited the manuscript.

Notes

The authors declare no competing financial interest.

ACKNOWLEDGMENTS

This research was supported by the National Natural Science Foundation of China under Projects 20973175, 21225104, 21171168, 21233009, and 21103190. We thank Prof. Ning Ye and Dr. Xin-Song Lin at FJIRSM for helping with the NLO property measurements, and Prof. Yong-Fan Zhang at Fuzhou University for helping with the NLO property calculations.

REFERENCES

(1) (a) Nikogosyan, D. N. *Nonlinear Optical Crystals: A Complete Survey*; Springer-Science: New York, 2005. (b) Wu, X.-T., Chen, L., Volume Eds. Structure−Property Relationships in Nonlinear Optical Crystals II The IR Region. In *Structure and Bonding*; Mingos, D. M., Series Ed.; Springer: New York, 2012; Vol. *145*.

(2) (a) Catella, G. C.; Shiozawa, L. R.; Hietanen, J. R.; Eckardt, R. C.; Route, R. K.; Feigelson, R. S.; Cooper, D. G.; Marquardt, C. L. *Appl. Opt.* **1993**, *32*, 3948. (b) Harasaki, A.; Kato, K. *Jpn. J. Appl. Phys.* **1997**, *36*, 700.

(3) Boyd, G. D.; Buehler, E.; Storz, F. G. *Appl. Phys. Lett.* **1971**, *18*, 301.

(4) (a) Petrov, V.; Yelisseyev, A.; Isaenko, L.; Lobanov, S.; Titov, A.; Zondy, J. J. *Appl. Phys. B: Laser Opt.* **2004**, *78*, 543. (b) Isaenko, L.; Yelisseyev, A.; Lobanov, S.; Titov, A.; Petrov, V.; Zondy, J. J.; Krinitsin, P.; Merkulov, A.; Vedenyapin, V.; Smirnova, J. *Cryst. Res. Technol.* **2003**, *38*, 379.

(5) Lin, X. S.; Zhang, G.; Ye, N. *Cryst. Growth Des.* **2009**, *9*, 1186.

(6) Yao, J. Y.; Mei, D. J.; Bai, L.; Lin, Z. S.; Yin, W. L.; Fu, P. Z.; Wu, Y. C. *Inorg. Chem.* **2010**, *49*, 9212.

(7) Petrov, V.; Badikov, V.; Shevyrdyaeva, G.; Panyutin, V.; Chizhikov, V. *Opt. Mater.* **2004**, *26*, 217.

(8) Knuteson, D. J.; Singh, N. B.; Kanner, G.; Berghmans, A.; Wagner, B.; Kahler, D.; McLaughlin, S.; Suhre, D.; Gottlieb, M. *J. Cryst. Growth* **2010**, *312*, 1114.

(9) Guo, S. P.; Wang, M. S.; Zou, J. P.; Zeng, H. Y.; Cai, L. Z.; Huang, J. S.; Guo, G. C. *Chem. Commun.* **2009**, 4366.

(10) Kim, Y.; Seo, I. S.; Martin, S. W.; Baek, J.; Halasyamani, P. S.; Arumugam, N.; Steinfink, H. *Chem. Mater.* **2008**, *20*, 6048.

(11) Chen, M. C.; Li, P.; Zhou, L. J.; Li, L. H.; Chen, L. *Inorg. Chem.* **2011**, *50*, 12402.

(12) Chen, M. C.; Li, L. H.; Chen, Y. B.; Chen, L. *J. Am. Chem. Soc.* **2011**, *133*, 4617.

(13) Yu, P.; Zhou, L. J.; Chen, L. *J. Am. Chem. Soc.* **2012**, *134*, 2227.

(14) (a) Lin, X. S.; Guo, Y. F.; Ye, N. *J. Solid State Chem.* **2012**, *195*, 172. (b) Yin, W. L.; Feng, K.; He, R.; Mei, D. J.; Lin, Z. S.; Yao, J. Y.; Wu, Y. C. *Dalton Trans.* **2012**, *41*, 5653.

(15) Chen, M. C.; Wu, L. M.; Lin, H.; Zhou, L. J.; Chen, L. *J. Am. Chem. Soc.* **2012**, *134*, 6058.

(16) Mei, D. J.; Yin, W. L.; Feng, K.; Lin, Z. S.; Bai, L.; Yao, J. Y.; Wu, Y. C. *Inorg. Chem.* **2012**, *51*, 1035.

(17) Zhao, H. J.; Zhang, Y. F.; Chen, L. *J. Am. Chem. Soc.* **2012**, *134*, 1993.

(18) Yin, W. L.; Feng, K.; Hao, W. L.; Yao, J. Y.; Wu, Y. C. *Inorg. Chem.* **2012**, *51*, 5839.

(19) Schwer, H.; Keller, E.; Kramer, V. *Z. Kristallogr.* **1993**, *204*, 203.

(20) Lin, H.; Zhou, L. J.; Chen, L. *Chem. Mater.* **2012**, *24*, 3406.

(21) *CrystalClear, version 1.3.5*; Rigaku Corp.: The Woodlands, TX, 1999.

(22) Sheldrick, G. M. *SHELXTL, version 5.1*; Bruker-AXS: Madison, WI, 1998.

(23) Spek, A. L. *J. Appl. Crystallogr.* **2003**, *36*, 7.

(24) Toby, B. H. *J. Appl. Crystallogr.* **2001**, *34*, 210.

(25) Kortüm, G. *Reflectance Spectroscopy*; Springer-Verlag: New York, 1969.

(26) Kurtz, S. K.; Perry, T. T. *J. Appl. Phys.* **1968**, *39*, 3798.

(27) (a) Kresse, G.; Furthmüller, J. *Phys. Rev. B* **1996**, *54*, 11169. (b) Perdew, J. P.; Wang, Y. *Phys. Rev. B* **1992**, *45*, 13244. (c) Kresse, G.; Joubert, D. *Phys. Rev. B* **1999**, *59*, 1758. (d) Blöchl, P. E. *Phys. Rev. B* **1994**, *50*, 17953. (e) Blöchl, P. E.; Jepsen, O.; Andersen, O. K. *Phys. Rev. B* **1994**, *49*, 16223.

(28) (a) Laksari, S.; Chahed, A.; Abbouni, N.; Benhelal, O.; Abbar, B. *Comput. Mater. Sci.* **2006**, *38*, 223. (b) Saha, S.; Sinha, T. P. *Phys. Rev. B* **2000**, *62*, 8828. (c) Mo, S. D.; Ching, W. *Phys. Rev. B* **1995**, *51*, 13023.

(29) (a) Rashkeev, S. N.; Lambrecht, W. R. L.; Segall, B. *Phys. Rev. B* **1998**, *57*, 3905. (b) Aversa, C.; Sipe, J. E. *Phys. Rev. B* **1995**, *52*, 14636.

(30) Kleinman, D. A. *Phys. Rev.* **1962**, *126*, 1977.

(31) Shannon, R. D. *Acta Crystallogr., Sect. A* **1976**, *32*, 751.

(32) O'Connor, C. *J. Prog. Inorg. Chem.* **1982**, *29*, 209.

(33) (a) Sanz, F.; Parada, C.; Rojo, J. M; Ruíz-Valero, C. *Chem. Mater.* **2001**, *13*, 1334. (b) Gao, E.-Q; Yue, Y.-F.; Bai, S.-Q; He, Z.; Zhang, S.-W; Yan, C.-H. *Chem. Mater.* **2004**, *16*, 1590. (c) Zhao, H. J; Li, L. H.; Wu, L. M; Chen, L. *Inorg. Chem.* **2010**, *49*, 5811.

(34) (a) Dmitriev, V. G.; Gurzadyan, G. G.; Nikogosyan, D. N. *Handbook of Nonlinear Optical Crystals*; Springer: New York, 1999. (b) Ebrahim-Zadeh, M.; Sorokina, I. T. *Mid-Infrared Coherent Sources and Applications*; NATO Science for Peace and Security Series B: Physics and Biophysics; Springer: New York, 2007.

(35) Bhar, G. C.; Smith, R. C. *Phys. Status Solidi A* **1972**, *13*, 157.

(36) (a) Kurtz, S. K.; Perry, T. T. *J. Appl. Phys.* **1968**, *39*, 3798. (b) Huang, Y.-Z.; Wu, L.-M.; Wu, X.-T.; Li, L.-H.; Chen, L.; Zhang, Y.-F. *J. Am. Chem. Soc.* **2010**, *132*, 12788.

(37) Zou, G. H.; Ye, N.; Huang, L.; Lin, X. S. *J. Am. Chem. Soc.* **2011**, *133*, 20001.

(38) Morris, C. D.; Chung, I.; Park, S.; Harrison, C. M.; Clark, D. J.; Jang, J. I.; Kanatzidis, M. G. *J. Am. Chem. Soc.* **2012**, *134*, 20733.

(39) (a) Godby, R. W.; Schluter, M.; Sham, L. J. *Phys. Rev. B* **1987**, *36*, 6497. (b) Okoye, C. M. I. *J. Phys.: Condens. Matter* **2003**, *15*, 5945.

(40) Lee, M.-H.; Yang, C.-H.; Jan, J.-H. *Phys. Rev. B* **2004**, *70*, 235110.